Flux Crystal Growth of Uranium(V) Containing Oxyfluoride Perovskites

Journal:	*Inorganic Chemistry Frontiers*
Manuscript ID	QI-RES-05-2019-000537.R2
Article Type:	Research Article
Date Submitted by the Author:	04-Sep-2019
Complete List of Authors:	Juillerat, Christian; University of South Carolina, Department of Chemistry and Biochemistry Kocevski, Vancho; University of South Carolina, Nuclear Engineering Program Morrison, Gregory; University of South Carolina, Chemistry and Biochemistry Karakalos, Stavros; University of South Carolina, College of Engineering and Computing Patil, Deepak; Alfred University, Materials Science & Engineering Misture, Scott; Alfred University, Materials Science & Engineering Besmann, Theodore; University of South Carolina, Nuclear Engineering Program Zur Loye, Hans-Conrad; University of South Carolina, Department of Chemistry and Biochemistry

Flux Crystal Growth of Uranium(V) Containing Oxyfluoride Perovskites

Christian A. Juillerat,[†§] Vancho Kocevski,[‡§] Gregory Morrison,[†§] Stavros G. Karakalos,[◊] Deepak Patil,[&] Scott T. Misture, [&] Theodore M. Besmann, [‡§] Hans-Conrad zur Loye,[*†‡]

[†]Department of Chemistry and Biochemistry, University of South Carolina, Columbia, SC, 29208, United States

[‡]Nuclear Engineering Program, University of South Carolina, Columbia, SC, 29208, United States

[§]Center for Hierarchical Wasteform Materials (CHWM), University of South Carolina, Columbia, SC, 29208, United States

[◊]Department of Chemical Engineering, University of South Carolina, Columbia, SC, 29208

[&]Kazuo Inamori School of Engineering, Alfred University, Alfred, NY, 14802, USA

Abstract:

The novel phases $Rb_4NaU_3O_{12-x}F_x$ (**1**), $K_4NaU_3O_{12-x}F_x$ (**2**), and $Rb_{2.1}K_{1.9}KU_3O_{12-x}F_x$ (**3**) were synthesized by molten flux methods using mixed alkali fluoride melts. The oxyfluorides crystallize in the cubic space group *Im-3m* with *a* lattice parameters of 8.7472(2) Å, 8.6264(2) Å, and 8.8390(3) Å, respectively. All three structures crystallize in a cubic perovskite structure, ABO_3 ($A_4BB'_3O_{12}$), where the A site is fully occupied by an alkali cation, and the B site is shared by the remaining smaller alkali cation and uranium in an ordered fashion such that the alkali cation on the B site is surrounded by square uranyl bipyramids. The structures were characterized by single crystal X-ray diffraction, energy dispersive spectroscopy, X-ray absorption near edge structure spectroscopy, X-ray photoelectron spectroscopy, magnetic susceptibility measurements, DFT calculations, thermogravimetric analysis, and UV-vis spectroscopy, all of which support the presence of U(V) in the three new materials.

Introduction:

The exploration of uranium crystal chemistry continues as nuclear technologies continue to receive attention in order to improve the nuclear fuel cycle, develop environmental remediation projects, and establish waste-forms to effectively immobilize waste radioisotopes and prevent migration of radionuclides in the environment.[1] The recent review on the flux crystal growth of uranium oxides emphasizes the contributions of the flux crystal growth technique in expanding the number of known uranium extended structures, and thus our understanding of uranium crystal chemistry. In particular, it brings attention to the abundance of U(VI) containing compounds, the readily achievable incorporation of U(IV) by using reducing reaction conditions, and the sparse examples of U(V) containing structures grown by flux methods. Specifically, out of the 180 structures in the review, 22 contain U(IV), only two contain solely U(V), and two contain mixed U(V/VI).[2] Uranium (V) chemistry is still relatively undeveloped, as reaction conditions that are conducive to incorporating this species into extended structures remain poorly understood; however, recent publications highlight the use of hydrothermal methods as an effective approach to target U(V) containing structures.[3, 4] Given these realities, it was a welcome surprise that we were able to grow three new uranium (V) containing structures from molten alkali fluoride fluxes using UF_4 as the uranium precursor in vessels open to the atmosphere. In our experience, starting with UF_4 in similar reaction conditions open to air has led to the complete oxidation of U(IV) to U(VI), resulting in U(VI) containing oxide structures.[5–12] One thus speculates if the presence of fluorine in these perovskite oxyfluorides can play a role in stabilizing the 5+ oxidation state of uranium.

The three reported U(V) containing structures, $Rb_4NaU_3O_{12-x}F_x$ (**1**), $K_4NaU_3O_{12-x}F_x$ (**2**), and $Rb_{2.1}K_{1.9}KU_3O_{12-x}F_x$ (**3**) adopt a cubic quadruple perovskite structure of the type $A_4BB'_3O_{12}$. In general, the highly adaptable ABO_3 perovskite structure consists of corner sharing BO_6 octahedra that create a central cavity in which the large A cation is located in a 12-fold coordination environment. [13] The perovskite structure readily accommodates a wide range of elements, including mixed site occupancies, and almost any property can be found for some perovskite composition, including a broad range of magnetic behaviors, such as ferro- and antiferromagnetism as well as, sometimes, superconductivity.

The perovskite family is versatile and contains numerous structural variants beyond the simple ABO_3 composition and even beyond the more complex quadruple perovskite structure $A_4BB'_3O_{12}$ mentioned above. [14] Specifically, the ABO_3 perovskite can be expanded into a double perovskite, where a third site is introduced, either as an A' or B' site, $A_2BB'O_6$, and this double perovskite structure, like the ABO_3 structure, can exhibit numerous structural distortions depending on the sizes of the A and B cations. More complex hexagonal/trigonal structures, such as the triple perovskite $A_3BB'_2O_9$[15] and quadruple perovskite $A_4BB'_3O_{12}$,[16] as well as an extensive family of 2H-perovskite related structures, $A_{3n+3m}A'_nB_{3m+n}O_{9m+6n}$ are all known for a wide variety of compositions and exhibit unique structural variations.[17]

The simple $A_2BB'O_6$ double perovskite's B and B' (or A and A') sites can be ordered in three distinct ways, rock-salt (Ba_2LnUO_6),[18] columnar ($NdSrMn^{3+}Mn^{4+}O_6$), or layered (La_2CuSnO_6).[19] If the ratio of B to B' is not 1:1 as in the example of the double perovskite, but rather 3:1, the perovskite family can be extended into either trigonal/hexagonal or cubic quadruple perovskites with the general formula $A_4BB'_3O_{12}$; the latter case being observed in the family of cubic structures reported in this paper. As one may imagine the cubic quadruple perovskite structure can also display ordering schemes similar to the double perovskite, although there are more possibilities and they are not as simple to describe as in the case of the double perovskites, and thus are beyond the scope of this paper. [20–22]

In addition to perovskites being a rewarding structural family to investigate for magnetic properties, modeling the magnetism arising from the unpaired electron in U(V)-containing perovskite structures is simplified in standard theoretical treatments due to the absence of 5f-5f electron repulsion effects that are of the same magnitude as spin-orbit coupling energies. Although studies on magnetic properties of U(V) oxides are few due to the small number of reported U(V) containing materials, there are in fact a small number reported for U(V) perovskites, namely the simple ternary AUO_3 (A = Na, K, Rb) family, and complex rare earth uranium oxides, e.g., Ba_2LnUO_6 (Ln = La, Nd, Sm). [3, 4, 18, 23–27] KU^VO_3 and RbU^VO_3 crystallize in the cubic perovskite structure while NaU^VO_3 crystallizes in a distorted orthorhombic structure type due to the smaller size of the sodium ion. In contrast, Ba_2LnUO_6 crystallizes in the double perovskite structure with rock salt type ordering of the Ln and U containing octahedra. The three compositions reported herein should be considered cubic quadruple perovskites with complex ordering of the Na (or K) and U containing octahedra, and partial substitution of oxygen by fluorine. Herein the synthesis, crystal structure and physical property measurements for these three compositions are presented.

Experimental

Materials and methods

UF_4 (International Bio-Analytical Industries, powder, ACS grade), $AlPO_4$ (Alfa Aesar, powder, 99.99%), RbF (Strem Chemicals, powder, 99.8%), KF (Alfa Aesar, 99%), and NaF (Alfa Aesar, powder, 99%) were used as received. ***Caution!*** *Although the uranium precursor used contained depleted uranium, standard safety measures for handling radioactive substances must be followed.*

The title compounds were synthesized by molten flux methods using a mixed alkali fluoride flux. For each reaction, 0.5 mmol UF_4, 0.2 mmol $AlPO_4$, and a 20 mmol mixture of RbF/NaF (0.65/0.35), RbF/KF (0.6/0.4), or KF/NaF (0.6/0.4) were loaded into platinum crucibles covered with lids and heated to 875 ^oC in 1.5 h, held for 12 h, and cooled to 600 ^oC at 6 ^oC/h. The bright red cubic crystals (Figure 1) were obtained in good yield (>80% based on uranium) and were separated from the flux by sonicating in water to dissolve the salt and isolated by vacuum filtration. Crystals were hand-picked to separate them from a small amount of an unidentified, poorly crystalline colorless product to obtain a phase pure sample.

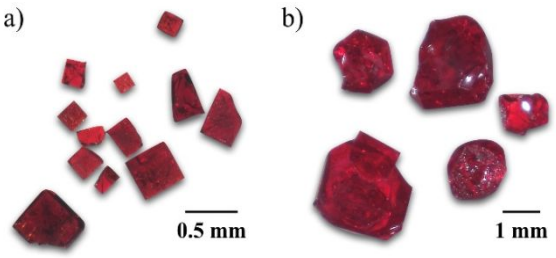

Figure 1: Optical images of crystals of a) $K_4NaU_3O_{12-x}F_x$ and b) $Rb_4NaU_3O_{12-x}F_x$.

Powder diffraction data were collected on a Bruker D2 Phaser equipped with an LYNXEYE silicon strip detector and a Cu Kα source to confirm the phase purity of the ground crystalline samples. EDS was used to verify the elemental compositions of the title compounds both on single crystals used for structure solution and bulk powders. EDS data were collected on a TESCAN Vega-3 SBU equipped with an EDS detector.

X-ray Absorption Near Edge Spectroscopy (XANES)

XANES data were collected on the title samples $Rb_4NaU_3O_{12-x}F_x$ (**1**), $K_4NaU_3O_{12-x}F_x$ (**2**), and $Rb_{2.1}K_{1.9}KU_3O_{12-x}F_x$ (**3**) in addition to $NaU^{V}O_3$, $U^{IV}O_2$, and $Sr_3U^{VI}O_6$, which were used as standards for the various uranium oxidation states. Samples for measurement were ~4 mg thin powder compacts in a double containment cell, with Kapton tape serving as the primary containment with a polymer bag as a second enclosure. The measurements were made at Beamline 10BM A, B at the Advanced Photon Source (APS) at Argonne National Laboratory in transmission mode near the uranium L_3-edge (17.1663 keV) with a yttrium foil K-edge (17.0384 keV) filter and a beam spot size of 2000 μm. Nine scans were collected for each sample, with the data sets averaged and normalized using ATHENA software. [28]

X-ray photoelectron spectroscopy (XPS)

X-ray photoelectron spectroscopy measurements were performed on powdered samples using a Kratos AXIS Ultra DLD XPS system with a hemispherical energy analyzer and a monochromatic Al Kα source operated at 15 keV and 150 W. The X-rays were incident at an angle of 45° with respect to the surface normal. Analysis was performed at a pressure below $1x10^{-9}$ mbar. High resolution core level spectra were measured with a pass energy of 40 eV. The XPS experiments were performed while using an electron gun directed on the sample for charge neutralization. Measurements were performed on both the as-prepared sample and after ion sputtering performed by accelerating Ar^+ ions (4 kV, 15 mA emission) towards the surface, as utilized in XPS analysis of other U(V) perovskites.[29]

Single-crystal X-ray diffraction (SXRD)

The structure of each compound was determined by single-crystal X-ray diffraction (SXRD) using a Bruker D8 Quest single crystal X-ray diffractometer equipped with a Mo Kα microfocus source

(λ = 0.71073 Å). The programs SAINT+ and SADABS within the APEX 3 software were used to perform the absorption correction. [30] The structure was solved using an intrinsic phasing solution method, SHELXT, and SHELXL was used to perform least-square refinements. [31, 32] Both SHELXT and SHEXL were used within the Olex 2 GUI. [33] Full sets of crystallographic values are listed in Table 1. Structure solutions for all three compounds were straightforward as they all crystallize in the cubic *Im-3m* space group and the asymmetric unit contains five unique sites in the analogous structures, U1, A1, A2, O1, and O2/F2 which occupy special positions and are assigned to Wyckoff sites 6b, 8c, 2a, 12d, and 12e, respectively. Note that for the $A_4BB'_3O_{12}$ structure type, A corresponds to the A1 site, B corresponds to the A2 site, and B' corresponds to the U1 site. The A1 sites are occupied by Rb, K, and mixed Rb/K and A2 sites are occupied by Na, Na, and K in structures **1**, **2**, and **3** respectively. All metal sites show no deviation from full occupancy when allowed to vary in refinements, except for the A1 site in **3**, which refines as 1.6 when modeled as a K and 0.73 when modeled as a Rb site, therefore it is best modeled as a mixture of the two, and freely refines to 47% K and 53% Rb. Assignment of the O1 and O2 sites as 100% occupied in all structures leads to a formula of $A_4NaU_3O_{12}$ and, in the highest oxidation state of U(VI), this formula does not charge balance having one residual negative charge. The X-ray scattering factors for fluorine and oxygen are negligibly different, and X-ray diffraction data is not sufficient for determining the ratio of oxygen to fluorine on the O2 sites. Fluorine was positively identified by EDS and XPS and the O2 site was fixed to F and O occupancies of 16.7% and 83.3%, respectively. No fluorine was modeled on the uranyl oxygen O1 site, as it is unlikely fluorine would form these stronger 'yl' bonds. The set occupancies of O and F on the O2 site slightly effect the free refinement of the Rb/K A2 site in structure **3** and introduce an uncertainty of 3%. While we choose to report the structures in this paper as $Rb_4NaU_3O_{12-x}F_x$ ($1 \leq x \leq 4$) due to the uncertainty in the fluorine content, the crystallographic files reflect compositions of $A_5U_3O_{11}F$ as the XANES results suggest the samples are predominantly U(VI).

Table 1: Crystallographic values for $Rb_4NaU_3O_{12-x}F_x$ (**1**), $K_4NaU_3O_{12-x}F_x$ (**2**), and $Rb_{2.1}K_{1.9}KU_3O_{12-x}F_x$ (**3**).

Compound	$Rb_4NaU_3O_{12-x}F_x$	$K_4NaU_3O_{12-x}F_x$	$Rb_{2.1}K_{1.9}KU_3O_{12-x}F_x$
	1	**2**	**3**
Space group	*Im-3m*	*Im-3m*	*Im-3m*
a (Å)	8.7472(3)	8.6264(2)	8.8390(3)
V (Å^3)	669.28(7)	641.93(3)	690.57(7)
Crystal size (mm^3)	0.02 x 0.04 x 0.08	0.02 x 0.02 x 0.02	0.02 x 0.02 x 0.02
Temperature (K)	302.01	296.5	302.01
Density (g cm^{-3})	6.366	5.678	5.777
θ range (deg)	3.294-36.265	3.340-36.247	3.259-36.219
μ (mm^{-1})	50.766	39.157	43.294
Collected reflections	2831	2752	2941
Unique reflections	191	188	198

R_{int}	0.0313	0.0258	0.0252
h	-14 < *h* < 11	-6 < *h* < 14	-14 < *h* < 13
k	-10 < *k* < 14	-10 < *k* < 10	-8 < *k* < 14
l	-9 < *l* < 14	-11 < *l* < 14	-11 < *l* < 14
$\Delta\rho_{max}$ (e Å^{-3})	0.919	0.550	0.487
$\Delta\rho_{min}$ (e Å^{-3})	-0.819	-1.067	-0.627
GoF	1.092	1.150	1.146
Extinction coefficient	0.00172(10)	--	0.00132(9)
$R_1(F)$ for $F_0^2>2\sigma(F_0^2)$[a]	0.0081	0.0086	0.0109
$R_w(F_0^2)$[b]	0.0231	0.0216	0.0228

[a] $R_1 = \Sigma||F_0| - |F_c||/\Sigma|F_0|$. [b] $wR_2 = [\Sigma w(F_0^2 - F_c^2)^2/\Sigma w(F_0^2)^2]^{1/2}$; $P = (F_0^2 + 2F_c^2)/3$; $w = 1/[\sigma^2(F_0^2) + (0.0128P)^2 + 1.0000P]$ for $Rb_4NaU_3O_{12-x}F_x$, $w = 1/[\sigma^2(F_0^2) + (0.0111P)^2 + 0.8022P]$ for $K_4NaU_3O_{12-x}F_x$, and $w = 1/[\sigma^2(F_0^2) + (0.0126P)^2]$ for $Rb_{2.1}K_{1.9}KU_3O_{12-x}F_x$.

Magnetic properties

Magnetic measurements were performed using a Quantum Design MPMS 3 SQUID magnetometer. Both field cooled (fc) and zero field cooled (zfc) measurements were performed over the temperature range of 2 K to 400 K under an applied magnetic field of 0.1 T. Magnetization measurements were also collected at 2 K, 50 K, and 300K by sweeping the applied magnetic fields between -5 and 5 T. Measurements were performed on both polycrystalline powders obtained by grinding single crystal products, and on samples consisting of many single crystals. The raw data were corrected for radial offset and shape effects following the method described by Morrison and zur Loye.[34]

Optical properties

UV-vis diffuse reflectance measurements were made on powdered samples of all three compositions using a PerkinElmer Lambda 35 UV-vis scanning spectrophotometer equipped with an integrating sphere . The diffuse reflectance data were internally converted to absorbance using the Kubelka-Munk equation and normalized.[35]

Thermal properties

Thermogravimetric analysis (TGA) was performed on $Rb_4NaU_3O_{12-x}F_x$ using a SDT Q600 (TA instruments), to determine thermal stability in atmospheres of 4% H_2 in Ar and air. The samples were loaded in alumina crucibles and heated to 800 °C under 4% H_2 and to 1000 °C in air at a rate of 10 °C/min. An additional experiment was run to further examine weight changes due to oxidation or reduction, where the sample was heated under N_2 to 600 °C at 10 °C/min and allowed to stabilize at this temperature for 10 minutes before switching to 4% H_2 for 30 mins, and then to N_2 for 5 mins, then to air for 30 mins, followed by N_2 for 5 mins, and finally back to 4% H_2 for 30 mins. All samples were analyzed by PXRD after TGA.

First-principles calculations

Density functional theory (DFT) calculations were performed using the VASP (Vienna Ab-initio Simulation Package) pseudopotential code,[36, 37] using the projector augmented waves (PAW) method[38, 39] and generalized gradient approximation (GGA) of the exchange-correlation potential in the PBE form.[40] Spin-polarized calculations were performed, with 520 eV cut-off energy for the plane waves, and 10^{-6} eV energy convergence criterion. A 4×4×4 **k**-point mesh and 0.005 eV/Å force convergence criterion were used for the calculations. The ground state geometries at 0 K were obtained by relaxing the cell volume and atomic positions, while keeping the cubic cell shape. Considering the correlated nature of the uranium 5-*f* electrons, the DFT+*U* method[41] was employed with $U = 4.0$ eV and J = 0.0 eV. To model the O sites partially occupied with F atoms (12d Wycoff position), super quasi-random structures (SQS) were generated with the compositions $K_4NaU_3O_9F_3$, $Rb_2K_3U_3O_9F_3$, $Rb_4NaU_3O_9F_3$, $K_4NaU_3O_8F_4$, $Rb_2K_3U_3O_8F_4$, and $Rb_4NaU_3O_8F_4$ using the mcsqs code provided by the Alloy Theoretic Automated Toolkit (ATAT) toolkit.[42–45] The chosen compositions are used to study the oxidation of U(V) and its effect on the magnetic properties of the compounds, providing insight into the U(V) chemistry in oxyfluorides. The generated SQS have U atoms with only one, two and three F atoms as first nearest neighbors (FNN).

Results and discussion

Synthesis

As observed in previously reported flux crystal growth experiments,[9, 46] the reaction vessel plays an important role in the successful formation of the target products. $Rb_4NaU_3O_{12-x}F_x$ was initially synthesized using the same reagent amounts and RbF/NaF flux described in the experimental section contained in silver tubes measuring 5.7 cm tall by 1.2 cm in diameter and welded shut on one end, and covered loosely with a silver cap. The reaction resulted in a yield greater than 80% based on uranium; however, when this reaction was repeated using the KF/NaF flux, the desired $K_4NaU_3O_{12-x}F_x$ phase was not obtained, but rather a mixture of simple potassium uranates was isolated. Performing this reaction in a platinum crucible instead of a silver tube resulted in the desired product. The reason the potassium sodium product preferentially forms in platinum crucibles, but not in silver tubes, unlike the rubidium sodium composition which forms in either, is not apparent.

The addition of $AlPO_4$, despite the fact the product contains neither Al or P, proved necessary for good yield of the product, and some cases the formation of the product. In silver tube reactions without the $AlPO_4$, the rubidium sodium composition does not form at all, and in the platinum reaction vessel the yield is decreased to less than 50% and is accompanied by an amorphous orange-yellow powder. When using the KF/NaF flux in a platinum crucible, the $K_4NaU_3O_{12-x}F_x$ phase forms without the addition of $AlPO_4$, but the yield is also significantly lower, and the products consist of approximately half of the target product and approximately half poorly

crystalline yellow plates that could not be identified. The synthesis of the Rb/K phase was only attempted in a platinum crucible using a RbF/KF flux and, in the absence of $AlPO_4$, results in only an amorphous product. However, in the presence of $AlPO_4$ it forms the desired product along with another unidentified phase that crystallizes as red-orange plates that turn yellow after sonication in water.

The synthesis of $K_4NaU_3O_{12-x}F_x$ was attempted by traditional solid state routes in reaction vessels open to air using stochiometric amounts of UF_4, U_3O_8, KNO_3, and $NaNO_3$; both compositions of x = 1 (all U^{6+}) and x = 4 (all U^{5+}) were attempted. Stochiometric mixtures of neither the x = 1 or x = 4 lead to a phase pure product. Regardless of the length of time or the temperature , the target phase was always accompanied by formation of KUO_3F and/or $K_2U_2O_7$. It is interesting to note that solid state reactions using only U_3O_8, UF_4, or $(UO_2)(NO_3)_2$•6 H_2O resulted in predominantly $K_2U_2O_7$ formation, whereas reactions with UF_4 and U_3O_8 produced a cubic perovskite phase with lattice parameters matching the desired composition. Using an excess of NaF to avoid the competitive formation of $K_2U_2O_7$ over the target phase, $K_4NaU_3O_{12-x}F_x$, was also unsuccessful in producing phase pure $K_4NaU_3O_{12-x}F_x$. Mixed fluxes of CsF/NaF and CsF/KF were also tried in platinum crucibles in the presence of the $AlPO_4$ that had proved essential for the synthesis of the three title compounds, but the Cs containing analog could not be obtained, and instead the reaction resulted in $K_2U_2O_7$ and $Na_2U_2O_7$ as the major products.

Crystal structure

Compounds $Rb_4NaU_3O_{12-x}F_x$ (**1**), $K_4NaU_3O_{12-x}F_x$ (**2**), and $Rb_{2.1}K_{1.9}KU_3O_{12-x}F_x$ (**3**) all adopt the cubic quadruple perovskite structure $A_4BB'_3O_{12}$, where Rb, K, and Rb/K occupy the A site for compounds **1**, **2**, and **3**, respectively and Na (or K in the case of 3) and U occupy the B and B' sites, respectively (Figure 2c). The fact that the cubic structure is observed for all three compositions can be explained by calculating the Goldschmidt tolerance factor t, for these compositions. Using a weighted average for the ionic radius of the B site, t values of 1.00, 0.974, and 0.948 are obtained for**1**, **2**, and **3** respectively. These t factors are typical for cubic perovskites and, hence, it is expected that all three compositions crystallize in a cubic rather than in a distorted structure. In order to illustrate the ordering of the B and B' cation sites in the cubic quadruple perovskite structure, a cubic perovskite, i.e., KUO_3 is shown in Figure 2a, while a cubic rocksalt ordered double perovskite, $A_2BB'O_6$ is shown in Figure 2b and the cubic quadruple perovskite structure of $Rb_4NaU_3O_{12-x}F_x$, is shown in Figure 2c. In **1-3,** each B' (Na or K) octahedron is surrounded by six uranium polyhedra, and the square uranium bipyramids corner share to form infinite chains in all three crystallographic directions. This structure is similar to other uranium perovskites such as $K_4CaU^{VI}_3O_{12}$, $K_4SrU^{VI}_3O_{12}$, $BaK_4U^{VI}_3O_{12}$, and $K_9U^{VI}_6O_{22.5}$, which are all based on the same type of B and B' site ordering, and all crystallize in the cubic space group, *Im*-3*m*.[47–49] The uranium polyhedra exhibit a uranyl coordination environment with two short axial bonds of 1.903(3), 1.904(4), and 1.856(3) Å for **1**, **2**, and **3**, respectively and equatorial U-O bond lengths of 2.18680(8) Å, 2.15660(5) Å, and 2.20975(8) Å, respectively. While a uranyl

coordination environment for U(V) species has not been observed in the handful of U(V) perovskites that have been well characterized, AUO_3 (A = Na, K, Rb) and $Ba_2LnU^{V}O_6$ (Ln = La, Nd, Sm),[18, 23] uranyl coordination for U(V) species is often observed in other uranium extended structures. In the U(V) perovskites the U-O bonds lengths are between 2.124 Å and 2.33 Å. In general, the observed uranyl bonds for the title compounds are long for U(VI), where 1.8 Å is average and the values of 1.9 Å fit well into the range of observed uranyl oxygen bond lengths for U(V), ~1.9-2.1 Å.[39] However, it is not unusual to observe long uranyl bonds for U(VI) species in perovskites that range from 1.737 Å to 1.966 Å and the equatorial U-O bonds range from 2.083 Å to 2.464 Å.[47, 48, 50–54] The coordination environments of the U atoms in the title compounds do not give any insight as to the oxidation state of the U species. Bond valence sums (BVS) were determined for structures **1**-**3** using values of 2.074 and 0.554 for r_0 and B, respectively for U-O bonds and values of 1.966 and 0.37 for r_0 and B, respectively for U-F bonds.[55, 56] The bond valence sums were calculated using 11 oxygen and 1 fluorine per formula unit, to ensure that each U atom has two axial oxygens, and four equatorial anion sites that are 16.7% fluorine and 83.3% oxygen. This resulted in BVS values of 5.81, 5.99, and 5.92 for **1**, **2**, and **3**. The BVSs reasonably agree with the expected value of 6 for U^{VI} in these structures. It is important to note, however, that the BVSs are greatly dependent on the amount O and F on the O2 site and, as the amount of F increases, the BVS approach values closer to 5, thus BVS gives no insight into the oxidation state of U without knowing the quantitative ratio of F/O. We have used the values of 1/6 F and 5/6 O since XANES suggests U(VI) is predominant in these structures.

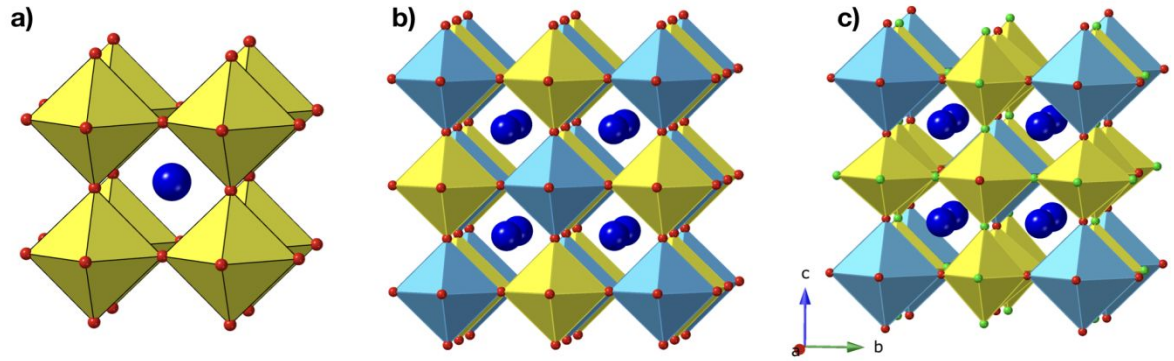

Figure 2: a) Cubic perovskite structure of KUO_3 b) cubic rock-salt ordered double perovskite, $A_2BB'O_6$, and c) cubic quadruple perovskite structure of $Rb_4NaU_3O_{12-x}F_x$ (**1**) where uranium polyhedra (B') are yellow, sodium octahedra (B) are light blue, rubidium atoms (A) are dark blue, oxygen atoms are red, and the mixed oxygen/fluorine sites are in green.

XANES

XANES is a useful technique to determine oxidation states because as the formal oxidation state, and thus the binding energy for exciting a core photoelectron increases, the transition energy shifts to higher energy. However, due to the fact the kinetic energy of the photoelectron is small in the XANES region, it is very sensitive to the chemical environment. Ideally, standards would have U

atoms in similar coordination environments—square bipyramids with shorter axial bonds and coordinate equatorially to four anions, where the anions are a mix of oxygen and fluorine. This is not possible to achieve given the limited library of known U(V) containing compounds, specifically in the UO_2^+ environment as U(V) is not ubiquitously found in the uranyl coordination, unlike U(VI), and the additional requirement of containing U-F bonds cannot be satisfied. $NaUO_3$ and Sr_3UO_6 standards were used for U(V) and U(VI), respectively, where U in these perovskite type structures adopts an octahedral coordination environment with bond distances of 2.142-2.151 Å and 2.061-2.098 Å, for $NaUO_3$ and Sr_3UO_6, respectively. Additionally, UO_2 was used as a U(VI) reference. The energies of the L_3 edge for all samples lie in the narrow region of 17173-17181 eV, where the standards progressively shift upfield as the U oxidation state increases (Figure 3b). The edge energies for compounds **1**-**3** lie between the reference samples $NaUO_3$ and Sr_3UO_6 where **1** and **2** are more upfield than **3** which features a different peak shape, perhaps due to the shorter axial bonds in **3** (1.856 Å) as compared to **1** and **2** (1.903 Å). For all three structures, the XANES results suggest the presence of both U(V) and U(VI), although the ratio of U(V)/U(VI) remains undetermined, due to the lack of proper U oxyfluoride reference materials. Few studies have been published on the effect of F substitution in uranium oxides on the shift in XANES edge transition energy; however, the work by Allen et al. shows that structures contain F have slightly lower transition energies than pure U(VI) oxides. [57–59] This could suggest that the F containing perovskites in this study contain more U(VI) than suggested by the comparison of the samples to the $NaUO_3$ and Sr_3UO_6 standards.

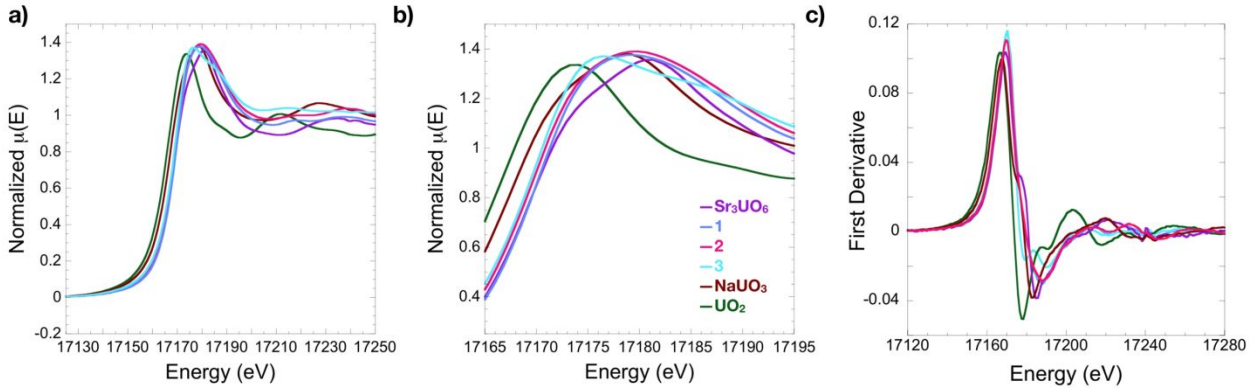

Figure 3: a) Normalized XANES spectra b) closer view of peaks in normalized XANES spectra and c) derivative normalized XANES spectra of $Rb_4NaU_3O_{12-x}F_x$ (**1**), $K_4NaU_3O_{12-x}F_x$ (**2**), and $Rb_{2.1}K_{1.9}KU_3O_{12-x}F_x$ (**3**) compared to reference samples of UO_2, $NaUO_3$, and Sr_3UO_6. The legend in b) applies to all three plots.

X-ray photoelectron spectroscopy

X-ray photoelectron spectroscopy measurements were performed on the as-prepared samples . Figure 4 shows the U 4f peaks of the corresponding materials after peak deconvolution, which indicated the presence of two U oxidation states. The presence of U(V) in the XPS spectra, indicates that after synthesis, at least part of the U in the material is in the U(V) oxidation state and

in all cases U(V) was measured to be ~10% of the total amount of U (Table 1). Taking into account that the XPS analysis depth is ~10nm and that ambient oxidation towards U(VI) takes place at the outermost atomic layers, the U(V) content in the bulk of the materials can be higher than the 10% measured by XPS on the surface of the sample. The quantification of the XPS spectra (Tables SI), confirmed the presence of fluorine in the structure, although the presence of adventitious carbon changed the expected surface atomic ratio.

Compound	$K_4NaU_3O_{12-x}F_x$	$Rb_4NaU_3O_{12-x}F_x$	$Rb_{2.1}K_{1.9}KU_3O_{12-x}F_x$
U^{6+} (%)	88.5	90.6	89.1
U^{5+} (%)	11.5	9.4	10.9

Table 1: The % ratio of U oxidation states recorded by XPS for each synthesized material.

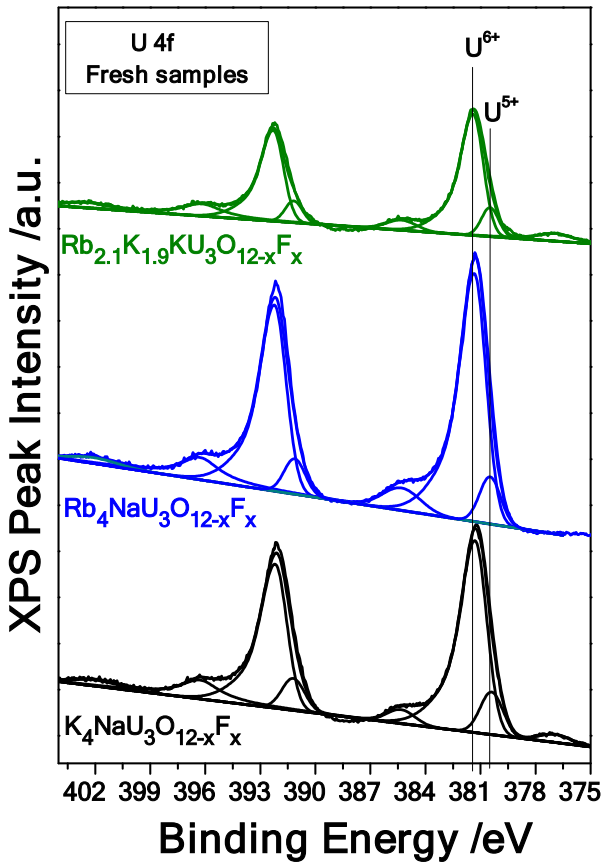

Figure 4: The U 4f XPS spectra of $K_4NaU_3O_{12-x}F_x$ (Black), $Rb_4NaU_3O_{12-x}F_x$ (Blue) and $Rb_{2.1}K_{1.9}KU_3O_{12-x}F_x$ (Green), measured after synthesis with no further treatment.

XPS studies on the U(V) perovskites, $NaUO_3$ and KUO_3, demonstrated that the satellite 4f peaks of U(V) could not be observed on as-prepared samples of $NaUO_3$ and KUO_3 due to surface

oxidation; however, short Ar sputtering times (20-30 sec) could remove the top most layer to reveal these satellite peaks which are considered "fingerprints" of a single U(V) chemical state.[4, 29] The etching time was critical, as too short a time did not completely remove the surface oxidation, while sputtering times of upwards of 60 sec reduced U(V) to U(IV). This study is highly relevant to the XPS study on U(V) containing perovskites, as similar methods were used with 30 sec of in-situ Ar^+ sputtering to remove contamination on the topmost atomic layer on the sample, including oxidation of the uranium, due to the exposure of the sample to the atmosphere. After sputtering, the four peak sequence named 1, 1', 2, 2' characteristic of a single U(V) chemical state was observed and is shown in Figure S2. The fact that the XANES data, which is a method that measures the response of the bulk sample, supports a predominantly U(VI) state, while the XPS after Ar sputtering suggest an entirely U(V) state could suggest that even the short 30 sec sputtering time was sufficient to reduce the U(VI) in the samples. Nevertheless, the presence of U(V) in the XPS spectra prior to sputtering confirm that a fraction of the U in the title materials is in the U(V) state. Further XPS experiments are needed on a variety of U(VI), U(V)/U(VI), and U(V) samples whose oxidation states can be confirmed be complimentary methods in order to explore the effects of Ar sputtering on the oxidation state of uranium.

Magnetic properties

Uranium V magnetism is not well understood despite the fact that it has only a single 5f electron, eliminating electronic 5f-5f repulsion interactions and simplifying experimental analysis. Many studies on U(V) structures yield moments much lower than the calculated 2.54 μ_B and often the experimental magnetism does not follow the Curie-Weiss law even at high temperatures, making the calculation of the moment more difficult.[18, 23, 27] The simple alkali perovskites, KUO_3 and $RbUO_3$, have been the subject of several magnetic studies reporting low moments of 0.2-0.66 μ_B determined using a modified Curie-Weiss law with a temperature independent susceptibility term.[23, 25–27, 60] Similarly, the magnetism of $Ba_2LnU^VO_6$ (Ln = La, Nd, Sm), which adopts a double perovskite structure, although monoclinically distorted, was reported to have a moment of 0.4 μ_B for the La composition, where a temperature independent susceptibility term was necessary to fit the data.[18] Besides the difference in cubic versus monoclinic symmetry in the KUO_3 and $Ba_2LaU^VO_6$ structures, the ordering of the uranium polyhedra is important to consider. In the cubic perovskite, KUO_3, U fully occupies the B site and therefore there are U-O-U linkages; however, in the double perovskite structure of $Ba_2LaU^VO_6$, the La and U sites order in a rock-salt fashion and all uranium polyhedra are isolated from each other. The magnetic data for both of these compositions represent an important comparison for title compounds, in which the uranium polyhedra form infinite chains; however, the ordered Na polyhedra set this structure apart from the simpler KUO_3 structure. Magnetic data for all three title compounds were collected on both powdered and single crystalline samples from 2 to 400 K in an applied field of 0.1 T and were found to exhibit low moments and non-Curie Weiss behavior even at high temperatures; however, the measurements of the magnitude of the moments was not repeatable on multiple samples of the same composition, and therefore a reliable moment for the U^{5+} ions could not be determined.

Similar measurements performed on $NaUO_3$ found that the raw moment of the title compounds is an order of magnitude smaller than $NaUO_3$, which agrees well with the ~10% U(V) estimated by XPS experiments. Differences between powder and single crystal samples were investigated for potential effects of surface oxidation; however, even measurements on separate single crystal samples produced magnetic moments of differing magnitudes. The inconsistency among multiple data sets for the same composition could not be attributed to impurities, as none were detected by powder diffraction (Figure 5), and may be attributed to inconsistent amounts of U(V) in the perovskite samples, as none of the methods used have been able to conclusively quantify the amount of U(VI) and U(V) in the title compounds. However, the presence of a small magnetic moment and non-Curie Weiss behavior is consistent with the presence of U(V) in the title compounds, especially, when compared to the reported magnetic data of KUO_3, $RbUO_3$, and $Ba_2LnU^{V}O_6$ (Ln = La, Nd, Sm). The magnetic susceptibility for $K_4NaU_3O_{12-x}F_x$ is shown in Figure S1.

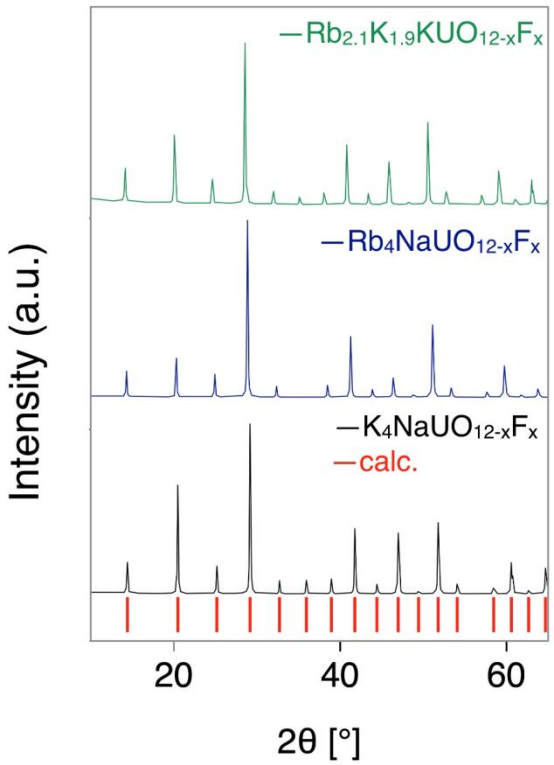

Figure 5: Powder diffraction data of $Rb_4NaU_3O_{12-x}F_x$ (blue), $K_4NaU_3O_{12-x}F_x$ (black), and $Rb_{2.1}K_{1.9}KU_3O_{12-x}F_x$ (green). The calculated peak positions for $K_4NaU_3O_{12-x}F_x$ are shown in red below the experimentally observed pattern of $K_4NaU_3O_{12-x}F_x$.

First-Principles Calculations

To better understand the influence of U-f interactions on magnetic behavior of the title compounds, their density of states (DOS) were calculated, see Figure 6. From the DOS it is evident that the states at the top of the valence band and bottom of the conduction band come from the U atoms,

indicating that these compounds are Mott insulators, just like UO_2. In the DFT calculations, the super quasi-random structures (SQSs) relaxed to states with 0 μ_B net magnetic moment, which agrees with the experimentally observed paramagnetic state of the title compounds. The DFT calculated band gaps of the $Rb_2K_2KU_3O_9F_3$, $Rb_4NaKU_3O_9F_3$ and $K_4NaU_3O_9F_3$ compounds are 2.866, 2.225 and 2.773 eV, respectively. Beside the apparent larger band gaps, the calculated and experimentally observed adsorption indexes show a similar shape with two distinct peaks, a large peak at lower energies and a smaller peak at higher energies.

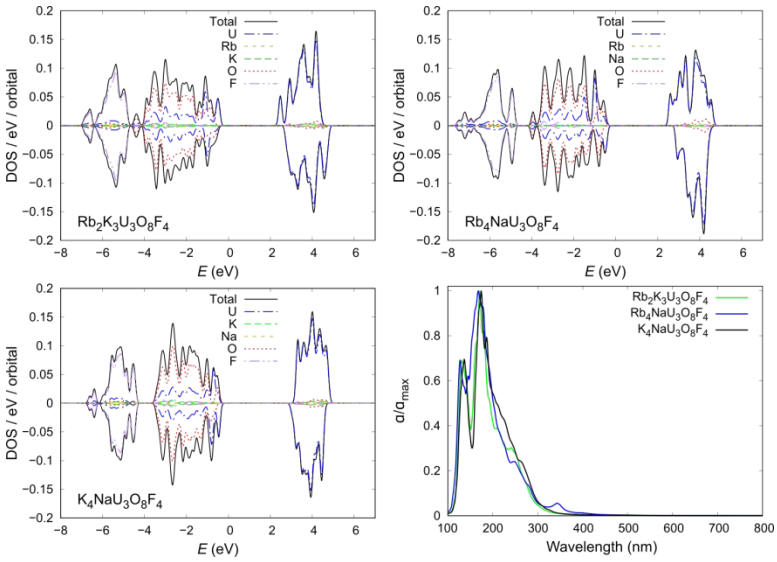

Figure 6. Density of states (DOS) of the $Rb_2K_2KU_3O_9F_3$ (top left), $Rb_4NaU_3O_9F_3$ (top right) and $K_4NaU_3O_9F_3$ (bottom left) compounds, and the U, Rb, K, Na, O, and F partial DOS. Adsorption indexes (bottom right) of the $Rb_2K_2KU_3O_9F_3$, $Rb_4NaU_3O_9F_3$, and $K_4NaU_3O_9F_3$ are shown in green, blue and black, respectively.

To better understand the low magnetic moments observed in the SQUID data and the possible effects of surface oxidation on bulk magnetic measurements, the magnetic moments of the U atoms were estimated in the $A_5U_3O_8F_4$ and $A_5U_3O_9F_3$ SQSs. They were estimated by integrating the spin-up and spin-down DOS up to the Fermi level. In the $A_5U_3O_8F_4$ SQSs all U atoms have |1| μ_B magnetic moment indicating that the U atoms have 1 unpaired electron, and hence are in the +5 oxidation states. However, two U atoms have -1 μ_B magnetic moment, while the other four U atoms have +1 μ_B magnetic moment, giving rise to a total of +2 μ_B of the SQSs of $A_5U_3O_8F_4$. On the other hand, the calculations show that the average oxidation state of the U atoms in the $A_5U_3O_9F_3$ SQSs is 5.33, where two of the U atoms do not have a magnetic moment, indicating that these U atoms are in the +6 oxidation state. The other four U atoms have +1 μ_B and -1 μ_B magnetic moment, implying that these U atoms have 1 unpaired electron and, hence, are in the +5 oxidation state. The magnetic moment of these four U atoms cancel each other to give the 0 μ_B net magnetic moment

of the SQSs. A closer look at the F atom coordination around the U atoms showed that U atoms with one, two and three F atoms FNN have 0, +1 and -1 μ_B magnetic moments, respectively. This is illustrated in Fig. 7, where the DOS of U with 1 F atom as a FNN are almost equal, while the spin-up and spin-down DOS are more dominant for the U with 2 and 3 F atoms as FNNs, respectively. While with the SQSs only a small portion is sampled of an otherwise complex structure of the title compounds, the results reinforce the fact that the random distribution of F atoms in the studied composition can yield a paramagnetic phase. Furthermore, the random distribution of the F atoms provides another reason for the varying paramagnetic SQUID data, although without experimental means of obtaining quantitative U(V)/U(VI) ratios it is impossible to identify the causes of the inconsistencies in the SQUID data.

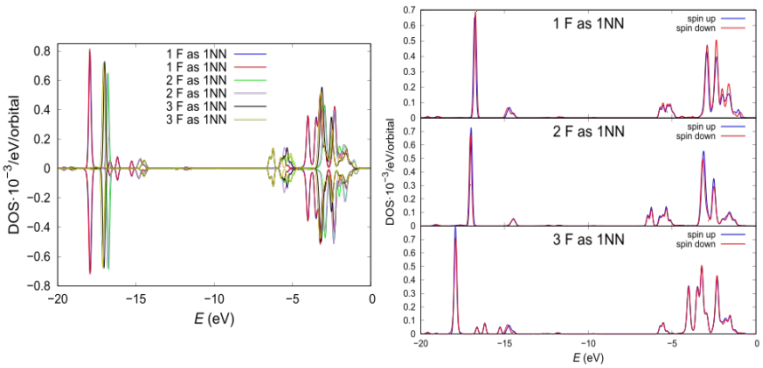

Figure 7. Left: projected density of states (pDOS) of the six U atoms in $Rb_2K_2KU_3O_9F_3$ compound. The pDOS of the two U atoms with 1, 2 and 3 F atoms as first nearest neighbor (FNN) are respectively shown in, blue and red, green and purple, and black and yellow. Right: comparison between the spin-up and spin-down pDOS of the U atoms with 1, 2 and 3 F atoms as FNN.

Thermal properties

Thermogravimetric analysis revealed that under a reducing atmosphere, $Rb_4NaU_3O_{12-x}F_x$ decomposes to $RbUO_3$ at 708 °C while it remains stable up to 1000 °C in air. Switching between these two atmospheres at a constant temperature of 600 °C results in mass changes of less than 0.3 wt % and cannot be attributed to either the complete oxidation of U^{5+} to U^{6+} or the complete reduction of U^{6+} to U^{5+} or U^{5+} to U^{4+}, as the weight change due to these processes is expected to be 1.9 wt %. Because XANES and XPS suggest predominantly U^{6+} with small amounts of U^{5+} and XPS showed that Ar sputtering easily reduces the U^{6+} in these samples to entirely U^{5+}, it would be reasonable to expect that under these conditions that the sample would show a larger weight change due to the reduction of U^{6+} to U^{5+}.

Optical properties

UV-vis diffuse reflectance data of the three title compounds display two broad bands centered at 430 nm and 540 nm (Figure 8). Reported U(VI) diffuse reflectance spectra[5–8, 61–63] contain two broad bands centered around ~350 nm and ~450 nm where the first feature arises from the equatorial ligand to metal charge transfer, and the second feature arises from the vibronically

coupled transitions of the UO_2^{2+} core.[3, 64] There are fewer examples of U(V) diffuse reflectance spectra in extended structures;[3, 4, 64] however, in those that are reported the U(V) charge transfer band is centered around 550 nm, as compared to a U(VI) charge transfer band of ~350 nm. By comparison, the spectra for **1-3** with bands centered at 430 nm and 540 nm are unusual for U(VI) species and could support the presence of U(V).

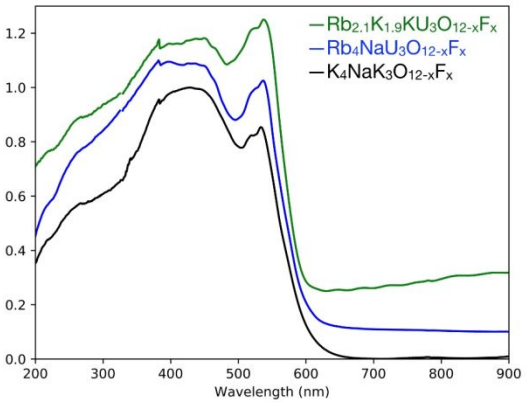

Figure 8: Normalized UV-vis absorption spectra of $Rb_4NaU_3O_{12-x}F_x$ (**1**), $K_4NaU_3O_{12-x}F_x$ (**2**), and $Rb_{2.1}K_{1.9}KU_3O_{12-x}F_x$ (**3**).

Conclusions

A series of U(V) containing oxyfluorides crystallizing in the perovskite structure, $Rb_4NaU_3O_{12-x}F_x$ (**1**), $K_4NaU_3O_{12-x}F_x$ (**2**), and $Rb_{2.1}K_{1.9}KU_3O_{12-x}F_x$ (**3**) were characterized by SXRD, PXRD, EDS, XANES, XPS, magnetic measurements, DFT calculations, TGA, and UV-vis diffuse reflectance spectroscopy. The structural characterization reveals square uranyl bipyramidal coordination environments. EDS and XPS both confirm the presence of fluorine, although neither provides a quantitative assessment of the fluorine content within the structure and there are no satisfactory methods to experimentally determine the F/O ratio or to investigate the F/O ordering. XANES data suggest the compounds are predominantly U(VI), while XPS, UV-vis, and magnetic data suggest small amounts of U(V) are present in the structure, although none of these methods have led to the quantification of the amounts of U(V) or U(VI). XPS estimates about 10% of U(V); however, the tendency for surface oxidation in U(V) species could lead to an underestimation of the content. PXRD confirms the phase purity of all samples. Magnetic measurements on multiple samples of all three compounds, powder and single crystalline, produced inconsistent small magnetic moments, but consistently showed non-Curie Weiss behavior, the presence of which supports the detection of small amounts of U(V) in all three materials. The DFT calculations reveal the importance of the F/O ordering in the $A_5U_3O_9F_3$ perovskite structure, where one, two, or three fluorine FNNs lead to magnetic moments of 0, 1, and -1 μB for the U atom in question, and thus the F/O ordering will have significant and possibly inconsistent effects (if there is only local rather than global ordering) on the average magnetic moment of the bulk material. The absence of the U(VI) charge transfer band at 350 nm in the UV-vis spectroscopy, and the appearance of bands

centered on 430 nm and 540 nm is unusual for U(VI) species and can support the presence of U(V). The difficulty of quantifying the amounts of U(VI) and U(V) in this structure illustrate the need for the development of new methods to do so, but also the need to further characterize U(V) and U(V) containing structures for comparison. The knowledge and understanding of U(V) containing structures in aspects of the synthesis, structural, magnetic, and optical characterization will continue to develop as new structures are synthesized and thoroughly characterized; a process in which this family of U(V) perovskites aids and enhances our understanding.

Acknowledgements

Research was conducted by the Center for Hierarchical Wasteform Materials (CHWM), an Energy Frontier Research Center (EFRC). Research was supported by the U.S. Department of Energy, Office of Basic Energy Sciences, Division of Materials Sciences and Engineering under Award DE-SC0016574. C. Juillerat is additionally supported by an NSF IGERT Graduate Fellowship under grant number 1250052. V. Kocevski and T. Besmann acknowledge the use computational resources provided by the National Energy Research Scientific Computing Center (NERSC) and the HPC cluster Hyperion, supported by The Division of Information Technology at University of South Carolina. XANES data collected on Beamline 10-BM-B at the Advanced Light Source, a U.S. Department of Energy (DOE) Office of Science User Facility operated for the DOE Office of Science by Argonne National Laboratory under Contract No. DE-AC02-06CH11357, and is directed by MRCAT and supported by the Department of Energy and the MRCAT member institutions.

References

(1) zur Loye, H.-C.; Besmann, T.; Amoroso, J.; Brinkman, K.; Grandjean, A.; Henager, C. H.; Hu, S.; Misture, S. T.; Phillpot, S.; Shustova, N. B.; Wang, H.; Koch, R. J.; Gregory Morrison; Dolgopolova, E., Hierarchical Materials as Tailored Nuclear Waste Forms: A Perspective, *Chem. Mater.* **2018**, *30*, 4475-4488.

(2) Juillerat, C. A.; Klepov, V. V.; Morrison, G.; Pace, K. A.; zur Loye, H.-C., Flux Crystal Growth: A Versatile Technique to Reveal the Crystal Chemistry of Complex Uranium Oxides, *Dalton Trans.* **2019**, *48*, 3162-3181.

(3) Pace, K. A., Klepov, V. V., Morrison, G., zur Loye, H.-C., "Moderate Supercritical Synthesis as a Facile Route to Mixed-Valent Uranium (IV/V) and (V/VI) Silicates", *Chem. Commun.*, **2018**, *54*, 13794-13797.

(4) Pace, K. A.; Kocevski, V.; Karakalos, S. G.; Morrison, G.; Besmann, T.; zur Loye, H.-C., $Na_2(UO_2)(BO_3)$: An All-Uranium(V) Borate Synthesized under Mild Hydrothermal Conditions, *Inorg. Chem.* **2018**, *57*, 4244-4247.

(5) Juillerat, C. A.; Moore, E. E.; Besmann, T. B.; zur Loye, H.-C., Observation of an Unusual Uranyl Cation-Cation Interaction in the Strongly Fluorescent Layered Uranyl Phosphates $Rb_6[(UO_2)_7O_4(PO_4)_4]$ and $Cs_6[(UO_2)_7O_4(PO_4)_4]$, *Inorg. Chem.* **2018**, *57*, 3675-3678.

(6) Juillerat, C. A.; Moore, E. E.; Morrison, G.; Smith, M. D.; Besmann, T. M.; zur Loye, H.-C., Versatile Uranyl Germanate Framework Hosting Twelve Different Alkali Halide 1D Salt Inclusions, *Inorg. Chem.* **2018**, *57*, 11606-11615.
(7) Juillerat, C. A.; Klepov, V. V.; Alekseev, E. V.; zur Loye, H.-C., Overstepping Löwenstein's Rule – a Route to Unique Aluminophosphate Frameworks with 3D Salt-Inclusion and Ion Exchange Properties, *Inorg. Chem.* **2019**, *58*, 724-736.
(8) Juillerat, C. A.; Moore, E. E.; Kocevski, V.; Besmann, T. M.; zur Loye, H.-C., A Family of Layered Phosphates Crystallizing in a Rare Geometrical Isomer of the Phosphuranylite Topology: Synthesis, Characterization, and Computational Modeling of $A_4[(UO_2)_3O_2(PO_4)_2]$ (A = alkali metals) Exhibiting Intra-layer Ion Exchange, *Inorg. Chem.* **2018**, *57*, 4726-4738.
(9) Juillerat, C. A.; zur Loye, H.-C., Crystal Growth and Structure Characterization of Three Layered Uranyl Phosphates and Their Relation to the Phosphuranylite Family, *Cryst. Growth Des.* **2019**, *19*, 1183-1189.
(10) Kocevski, V.; Juillerat, C. A.; Moore, E. E.; zur Loye, H.-C.; Besmann, T., Understanding the polymorphism of $A_4[(UO_2)_3(PO_4)_2O_3]$ (A=alkali metals) uranyl phosphate framework structures, *Cryst. Growth Des.* **2019**, *19*, 966-975.
(11) Morrison, G.; Smith, M. D.; zur Loye, H.-C., Understanding the Formation of Salt-Inclusion Phases: An Enhanced Flux Growth Method for the Targeted Synthesis of Salt-Inclusion Cesium Halide Uranyl Silicates, *J. Am. Chem. Soc.* **2016**, *138*, 7121-7129.
(12) Morrison, G.; Smith, M. D.; zur Loye, H.-C., Flux versus Hydrothermal Growth: Polymorphism of $A_2(UO_2)Si_2O_6$ (A = Rb, Cs), *Inorg. Chem.* **2017**, *56*, 1053-1056.
(13) Giaquinta, D. M.; zur Loye, H.-C., Structural predictions in the ABO_3 phase diagram, *Chem. Mater.* **1994**, *6*, 365-372.
(14) Stitzer, K. E., Darriet, J., zur Loye, H.-C., "Advances in the Synthesis and Structure Description of 2H-Hexagonal Perovskite Related Oxides", DOI:10.1016/S1359-0286(01)00032-8. *Curr. Opin. Solid State Mater. Sci.*, **2001**, *5*, 535-544.
(15) Stitzer, K.; Smith, M. D.; Gemmill, W. R.; zur Loye, H.-C., Novel mixed-valent (V/VI) triple perovskite ruthenates: Observation of a complex low-temperature structural and magnetic transition, *J. Am. Chem. Soc.* **2002**, *124*, 13877-13885.
(16) Ferreira, T.; Heald, S. M.; Smith, M. D.; zur Loye, H.-C., Unusual Coexistence of Nickel(II) and Nickel(IV) in the Quadruple Perovskite $Ba_4Ni_2Ir_2O_{12}$ Containing Ir_2NiO_{12} Mixed-Metal-Cation Trimers, *Inorg. Chem.* **2018**, *57*, 2973-2976.
(17) zur Loye, H.-C.; Zhao, Q.; Bugaris, D. E.; Chance, W. M., 2 H-perovskite related oxides: Synthesis, structures, and predictions, *CrystEngComm* **2012**, *14*, 23-39.
(18) Phatak, R.; Yadav, A. K.; Pathak, N.; Prajapat, C. L.; Kasar, U. M.; Singh, M. R.; Jha, S. N.; Bhattacharyya, D.; Das, A.; Sali, S. K., Pentavalent uranium complex oxides: A case study on double perovskites $Ba_2REU^{5+}O_6$ (RE = La, Nd, Sm), *J. Alloys Compd.* **2017**, *708*, 1168-1177.
(19) King, G.; Woodward, P. M., Cation ordering in perovskites, *J. Mater. Chem.* **2010**, *20*, 5785.
(20) Belik, A. A.; Khalyavin, D. D.; Zhang, L.; Matsushita, Y.; Katsuya, Y.; Tanaka, M.; Johnson, R. D.; Yamaura, K., Intrinsic Triple Order in A-site Columnar-Ordered Quadruple Perovskites: Proof of Concept, *ChemPhysChem* **2018**, *19*, 2449-2452.

(21) Belik, A. A.; Matsushita, Y.; Kumagai, Y.; Katsuya, Y.; Tanaka, M.; Stefanovich, S. Y.; Lazoryak, B. I.; Oba, F.; Yamaura, K., Complex Structural Behavior of $BiMn_7O_{12}$ Quadruple Perovskite, *Inorg. Chem.* **2017**, *56*, 12272-12281.
(22) Yin, Y. Y.; Liu, M.; Dai, J. H.; Wang, X.; Zhou, L.; Cao, H.; dela Cruz, C.; Chen, C. T.; Xu, Y.; Shen, X.; Yu, R.; Alonso, J. A.; Muñoz, A.; Yang, Y. F.; Jin, C.; Hu, Z.; Long, Y., $LaMn_3Ni_2Mn_2O_{12}$: An A- and B-Site Ordered Quadruple Perovskite with A-Site Tuning Orthogonal Spin Ordering, *Chem. Mater.* **2016**, *28*, 8988-8996.
(23) Van den Berghe, S.; Leenaers, A.; Ritter, C., Antiferromagnetism in MUO3 (M = Na, K, Rb) studied by neuron diffraction, *J. Solid State Chem.* **2004**, *177*, 2231-2236.
(24) Lin, C.; Chen, C.-S.; Shiryaev, A. A.; Zubavichus, Y. V.; Lii, K.-H., $K_3(U_3O_6)(Si_2O_7)$ and $Rb_3(U_3O_6)(Ge_2O_7)$: a pentavalent-uranium silicate and germanate, *Inorg. Chem.* **2008**, *47*, 4445-4447.
(25) König, E.; Rudowicz, C.; Desai, V. P.; Kanellakopulos, B., Low-temperature magnetism of some alkali metal uranates(V) and alkaline earth neptunates(IV). Examples for ferrimagnetism in mixed actinide oxides, *The Journal of Chemical Physics* **1983**, *78*, 5764-5771.
(26) Hinatsu, Y., Magnetic Susceptibility an Electron Paramagnetic Resonance Study of KUO_3 with cubic perovskite structure, *J. Solid State Chem.* **1994**, *1120*, 118-123.
(27) Hinatsu, Y.; Shimojo, Y.; Morri, Y., Magnetic and neutron diffraction studies on potassium uranate KUO_3, *J. Alloys Compd.* **1998**, *270*, 127-131.
(28) Ravel, B.; Newville, M., ATHENA, ARTEMIS, HEPHAESTUS: data analysis for X-ray absorption spectroscopy using IFEFFIT, *J. Synchrotron Rad.* **2005**, *12*, 537-541.
(29) Liu, J.-H.; Van den Berghe, S.; Konstantinovíc., XPS spectra of the U^{5+} compounds KUO_3, $NaUO_3$ and $Ba_2U_2O_7$, *J. Solid State Chem.* **2009**, *182*, 1105-1108.
(30) Bruker. *APEX3, SAINT+, and SADABS.* Bruker AXS Inc.: Madison, Wisconsin, USA, 2015;
(31) Sheldrick, G. M., Crystal structure refinement with SHELXL, *Acta Cryst.* **2015**, *C71*, 3-8.
(32) Sheldrick, G. M., SHELXT - Integrated space-group and crystal-structure determination, *Acta Cryst.* **2015**, *A71*, 3-8.
(33) Dolomanov, O. V.; Bourhis, L. J.; Gildea, R. J.; Howard, J. A. K.; Pushmann, H., OLEX2: a complete structure solution, refinement and analysis program, *J. Appl. Crystallogr.* **2009**, *42*, 339-341.
(34) Morrison, G.; zur Loye, H.-C., Simple correction for the sample shape and radial offset effects on SQUID magnetometers: Magnetic measurements on Ln_2O_3 (Ln=Gd, Dy, Er) standards, *J. Solid State Chem.* **2015**, *221*, 334-337.
(35) Kubelka, P.; Munk, F. Z., Ein Beitrag Zur Optik Der Farbanstriche, *Z. Techn. Phys.* **1931**, *12*, 593-601.
(36) Kresse, G.; Furthmuller, J., Efficient iterative schemes for ab-initio total-energy calculations using a plane-wave basis set, *Phys. Rev. B* **1996**, *54*, 11169-11186.
(37) Kresse, G.; Furthmuller, J., Efficiency of ab-initio total energy calculations for metals and semiconductors using a plane-wave basis set, *Comput. Mater. Sci.* **1996**, *6*, 15-50.
(38) Blöchl, P. E., Projector augmented-wave method, *Phys. Rev. B* **1994**, *50*, 17953-17979.
(39) Kresse, G.; Joubert, D., From ultrasoft pseudopotentials to the projector augmented-wave method, *Phys. Rev. B* **1999**, *59*, 1758-1775.
(40) Perdew, J. P.; Burke, K.; Ernzerhof, M., Generalized Gradient Approximation Made Simple, *Phys. Rev. Lett.* **1996**, *77*, 3865-3868.

(41) Dudarev, S. L.; Botton, G. D.; Savrasov, S. Y.; Humphreys, C. J.; Sutton, A. P., Electron-energy-loss spectra and the structural stability of nickel oxide: An LSDA+U study, *Phys. Rev. B* **1998**, *57*, 1505-1509.
(42) Walle, A., Multicomponent multisublattice alloys, nonconfigurational entropy and other additions to the Alloy Theoretic Automated Toolkit, *Calphad* **2009**, *33*, 266-278.
(43) Walle, A.; Ceder, G., Automating first-principles phase diagram calculations, *J. Phase Equilib.* **2002**, *23*, 521-538.
(44) Walle, A.; ASta, M.; Ceder, G., The alloy theoretic automated toolkit: A user guide, *CALPHAD: Comput. Coupling Phase Diagrams Thermochem.* **2002**, *26*, 539-553.
(45) Walle, A.; Asta, M., Self-driven lattice-model Monte Carlo simulations of alloy thermodynamic properties and phase diagrams., *Modell. Simul. Mater. Sci. Eng* **2002**, *10*, 521-538.
(46) Morrison, G.; zur Loye, H.-C., Flux Growth of $[NaK_6F][(UO_2)_3(Si_2O_7)_2]$ and $[KK_6Cl][(UO_2)_3(Si_2O_7)_2]$: The Effect of Surface Area to Volume Ratios on Reaction Products, *Cryst. Growth Des.* **2016**, *16*, 1294-1299.
(47) Read, C. M.; Bugaris, D. E.; zur Loye, H.-C., Single crystal growth and structural characterization of four complex uranium oxides: $CaUO_4$, β-Ca_3UO_6, $K_4CaU_3O_{12}$, and $K_4SrU_3O_{12}$, *Solid State Sci.* **2013**, *17*, 40-45.
(48) Roof, I. P.; Smith, M. D.; zur Loye, H.-C., Crystal growth of uranium-containing complex oxides: $Ba_2Na_{0.83}U_{1.17}O_6$, $BaK_4U_3O_{12}$ and $Na_3Ca_{1.5}UO_6$, *Solid State Sci.* **2010**, *12*, 1941-1947.
(49) Saine, M. C.; Gasperin, M.; Jove, J.; Cousson, A., Relation entre la structure cristalline d'un uranate de potassium $K_9U_6O_{22.5}$ et les spectres mössbauer (^{237}Np) des phases apparentées de neptunium, *J. Less-Common Met.* **1987**, *132*, 141-148.
(50) Read, C. M.; Smith, M. D.; zur Loye, H.-C., Single Crystal Growth and Structural Characterization of a Novel Mixed-Valent Ternary Uranium Oxide, $K_8U_7O_{24}$, *J Chem Crystallogr* **2014**, *44*, 604-608.
(51) Chernorukov, N. G.; Knyazev, A. V.; Dashkina, Z. S., Synthesis, structures, and physicochemical properties of $Sr_2A^{II}UO_6$(A^{II} = Mg, Ca, Sr, Ba, Mn, Fe, Co, Ni, Zn, and Cd) compounds, *Russian Journal of Inorganic Chemistry* **2010**, *55*, 904-912.
(52) Groen, W. A.; Ijdo, D. J. W., The monoclinic perovskites Sr_2CaUO_6 and Ba_2SrUO_6. A Rietveld refinement of neutron powder diffraction data, *Acta Cryst.* **1987**, *C43*, 1033-1036.
(53) Pinacca, R.; Viola, M. C.; Pedregosa, J. C.; Muñoz, A.; Alonso, J. A.; Martínez, J. L.; Carbonio, R. E., Crystal and magnetic structure of the double perovskite Sr_2CoUO_6: a neutron diffraction study, *Dalton Trans.* **2005**, 447-451.
(54) Pinacca, R. M.; Viola, M. C.; Pedregosa, J. C.; Martínez-Lope, M. J.; Carbonio, R. E.; Alonso, J. A., Preparation, crystal structure and magnetic behavior of new double perovskites Sr2B′ UO6 with B′= Mn, Fe, Ni, Zn, *J. Solid State Chem.* **2007**, *180*, 1582-1589.
(55) Burns, P. C.; Ewing, R. C.; Hawthorne, F. C., The crystal chemistry of hexavalent uranium: polyhedron geometries, bond-valence parameters, and polymerization of polyhedra, *Can. Mineral.* **1997**, *35*, 1551-1570.
(56) Brese, N. E.; O'Keeffe, M., Bond-Valence Parameters for Solids, *Acta Cryst.* **1991**, *B47*, 192-197.

(57) Allen, S.; Barlow, S.; Halasyamani, P. S.; Mosselmans, J. F. W.; O'Hare, D.; Walker, S. M.; Walton, R. I., Hydrothermal Synthesis of $(C_6N_2H_{14})_2(U^{VI}_2U^{IV}O_4F_{12})$, a Mixed-Valent One-Dimensional Uranium Oxyfluoride, *Inorg. Chem.* **2000**, *39*, 3791-3798.
(58) Kosog, B.; La Pierre, H. S.; Denecke, M. A.; Heinemann, F. W.; Meyer, K., Oxidation state delineation via U L_{III}-edge XANES in a series of isostructural uranium coordination complexes., *Inorg. Chem.* **2012**, *51*, 7940-7944.
(59) Sanyal, K.; Khooha, A.; Das, G.; Tiwari, M. K.; Misra, N. L., Direct Determination of Oxidation States of Uranium in Mixed-Valent Uranium Oxides Using Total Reflection X-ray Fluorescence X-ray Absorption Near-Edge Spectroscopy., *Anal. Chem.* **2017**, *89*, 871-876.
(60) Kanellakopulos, B.; Henrich, E.; Keller, C.; Baumgärtner, F.; König, E.; Desai, V. P., Optical spectra and magnetism between 4.2 and 300 K for some alkali metal and alkaline earth metal uranates(V), neptunates(VI), and a plutonate(VII), *Chem. Phys.* **1980**, *53*, 197-213.
(61) Morrison, G.; Smith, M. D.; Tran, T. T.; Halasyamani, S.; zur Loye, H.-C., Synthesis and structure of the new pentary uranium(VI) silicate, $K_4CaUSi_4O_{14}$, a member of a structural family related to frenoite, *CrystEngComm* **2015**, *17*, 4218-4224.
(62) Read, C. M.; Yeon, J.; Smith, M. D.; zur Loye, H.-C., Crystal growth, structural characterization, cation–cation interaction classification, and optical properties of uranium (vi) containing oxychlorides, $A_4U_5O_{16}Cl_2$ (A= K, Rb), $Cs_5U_7O_{22}Cl_3$, and AUO_3Cl (A=Rb, Cs), *CrystEngComm* **2014**, *16*, 7259-7267.
(63) Juillerat, C. A.; Kocevski, V.; Besmann, T.; zur Loye, H.-C., Observation of the Same New Sheet Topology in Both the Layered Uranyl Oxide-Phosphate $Cs_{11}[(UO_2)_{12}(PO_4)_3O_{13}]$ and the Layered Uranyl Oxyfluoride-Phosphate $Rb_{11}[UO_2)_{12}(PO_4)_3O_{12}F_2]$ Prepared by Flux Crystal Growth, DOI:10.3389/fchem.2019.00583. *Frontiers in Chemistry*, **2019**, *7*, article 583.
(64) Stritzinger, J. T.; Alekseev, E. V.; Polinski, M. J.; Cross, J. N.; Eaton, T. M.; Albrecht-Schmitt, T. E. L. M. C. T., Further Evidence for the Stabilization of U(V) within a tetraoxo Core, *Inorg. Chem.* **2014**, *53*, 5294-5299.

For Table of Contents Use Only

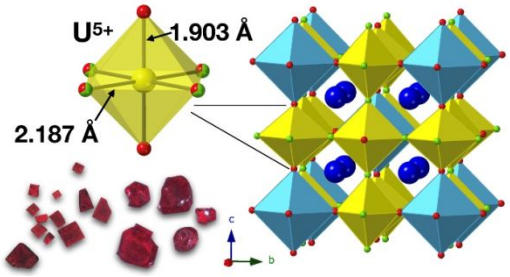

Synopsis: Crystals of three new uranium(V) containing oxyfluorides were grown using an alkali fluoride flux and adopt an ordered quadruple perovskite structure.